Anisotropic magnetism of graphite irradiated with medium-energy hydrogen and helium ions

T. L. Makarova* and A. L. Shelankov
Department of Physics, Umeå University, Umeå, Sweden, and Ioffe Physico-technical Institute of the RAS, St. Petersburg, Russia

I. T. Serenkov and V. I. Sakharov
Ioffe Physico-technical Institute of the RAS, St. Petersburg, Russia

D. W. Boukhvalov
Computational Materials Science Center, National Institute for Materials Science, 1-2-1 Sengen, Tsukuba, Ibaraki 305-0047, Japan
(Received 20 July 2010; revised manuscript received 17 October 2010; published 18 February 2011)

We have studied the changes in the magnetic behavior of highly oriented pyrolytic graphite (HOPG) samples subjected to medium-energy proton and helium irradiation. The variations of the ferromagneticlike magnetization curves with the irradiation dose have been studied for two configurations: magnetic fields parallel and perpendicular to graphitic planes. For high irradiation doses, the values of magnetization at saturation are close for both geometries. At low irradiation fluences an orientationally dependent magnetic response is obtained. Directional dependence of magnetization indicates that the magnetism in irradiated graphite is triggered by vertically aligned intrinsic carbon defects induced by irradiation. This physical picture has been verified by the observation of a local stray field near linear defects by means of magnetic force microscopy. Similar results obtained with hydrogen and helium ions confirm that the chemical nature of projectiles is not crucial for formation of ferromagnetic order in oriented graphite. The dependence of induced magnetic moment versus irradiation dose shows a maximum; the optimal dose is an order of magnitude less for helium ions than for protons, being in line with simulations showing that He^+ generates 8 times more defects than H^+. Raman studies indicate that the degradation of magnetic ordering at large irradiation doses occurs much earlier than graphite amorphization but coincides with the destruction of graphene sheet stacking.

DOI: 10.1103/PhysRevB.83.085417 PACS number(s): 78.70.−g, 75.50.Dd, 78.30.Ly, 68.37.Rt

I. INTRODUCTION

Magnetism in systems that do not contain transition metal or rare earth ions is an intriguing topic in modern condensed matter physics.[1–3] Besides its importance for fundamental physics, this field area has a great potential for applications. As it has been recently realized, carbon-based materials, which show magnetic activity,[4] are very promising for spintronics.[5,6] It has been found that local magnetism in highly oriented pyrolytic graphite (HOPG) arises at the grain boundary regions which propagate along the c axis of the graphite crystal, creating two-dimensional planes of defects[7] whereas in graphene magnetic species with $\mu \approx 4$–$5\ \mu_B$ were detected,[8] suggesting that magnetic ordering is unlikely to arise without involvement of three-dimensional interactions. Whereas a rich variety of magnetism scenarios in carbon nanostructures have been proposed (Ref. 9 and references therein), there are far more questions than answers on the experimental side of the field. Magnetization values for pristine HOPG do not exceed 2×10^{-3} A m^2 kg^{-1} at room temperature.[7,10] For this phenomenon to find useful applications it is necessary to considerably increase magnetization values.

Ion implantation is a relatively easy method for inducing magnetism in graphite.[11] Irradiation-induced magnetism has been attributed to carbon π-electron systems.[12] Therefore vacancies,[13–15] interstitials,[16–18] edges,[19–21] adsorption defects,[22] hydrogen complexes with vacancies or adatoms,[23–25] and other types of disorder[26,27] have been regarded as sources for creating unpaired carbon atoms in the lattice. Still, there is a lack of clarity whether the chemical nature of projectiles is of importance, since successful experiments were reported for hydrogen,[11,28] nitrogen,[28] and carbon,[28,29] whereas implantations with iron,[30,31] boron and fluorine,[31] and helium[32–34] were reported not to trigger magnetic ordering. Some problems concern the reproducibility of the experiments with the MeV-proton bombardment: the magnetic data[11] were confirmed by subsequent publications,[28,30–33,35,36] but in other groups[34,37] only paramagnetic response was registered. The controversy of experimental data hinders physical interpretation of irradiation-induced magnetism.

In this communication, we present results of magnetic measurements on highly oriented pyrolytic graphite bombarded with medium energy protons and helium ions at various doses of the irradiation. We observe that for the low irradiation doses saturation magnetization turns out to be even higher for helium ion irradiation than for hydrogen ion irradiation, suggesting that the emergence of magnetic ordering is determined by the processes of defect formation. The samples show ferromagneticlike behavior with a pronounced anisotropy of the irradiation-induced magnetization. The anisotropy is evident at low irradiation doses whereas at high fluences magnetic properties become essentially isotropic, in agreement with previously published results. Magnetic force microscopy studies indicated the location of magnetically active regions, whereas Raman spectroscopy revealed the occurrence of some structural changes which could be associated with the vanishing of magnetism at high irradiation doses. As we discuss later, these observations allow us to make a conjecture concerning the origin of magnetism.

II. EXPERIMENT

We studied irradiation effects on ten samples of HOPG from Advanced Ceramics. The samples were irradiated at room temperature by a broad beam of medium energy (225 keV) H^+ and He^+ ions on a total area of 2 mm^2 at an ion current of 2 nA. The irradiation doses were in the range 1×10^{15} to 1×10^{17} ion/cm^2. The bombardment with comparatively low-energy ions at a weak ion current does not overheat the samples, thus preventing unwanted relaxation effects (like those observed during high-energy ion bombardment[28]). According to our estimates, the sample temperature during the irradiation does not exceed 50–80 °C for these beam parameters.

An impurity analysis of the pristine HOPG (ZYA grade) samples, performed by high-resolution inductive coupled plasma mass spectrometry (HR ICP MS), showed that the concentrations of Co, Cr, Fe, Mn, and Ni were 0.0121, 0.0299, 1.33, 0.03, and 0.400 mg/kg, respectively, with 15% uncertainty. The magnetic measurements completed, elemental composition of the samples was analyzed again with particle-induced x-ray emission (PIXE). The analysis verified that irradiation as well as sample handling did not introduce impurities: Only six elements were above the limit of detection for PIXE in the irradiated samples, namely, Ca, Ti, Mn, Fe, Cu, and Zn with concentrations of 4.0 (1.6), 1.3 (0.9), 0.6 (0.5), 1.0 (0.4), 0.4 (0.3), and 0.4 (0.3) mg/kg. The values in parentheses stand for the limit of detection. Thus, the total content of metallic impurities which could be responsible for unwanted extrinsic magnetic effects was below 1 elemental ppm. For the samples which were about 1 mg in weight, maximum possible contribution of the impurities to the magnetic moment can be estimated as 0.3×10^{-6} emu, assuming a parallel alignment of the impurity moments. The magnetic moments reported here are in the range 2–25 $\times 10^{-6}$ emu, thus surpassing possible parasitic effects by almost 2 orders of magnitude. The magnetic measurements were carried out with a Quantum Design MPMS XL-1 SQUID magnetometer using the reciprocating sample option. M(H) data were collected with the external field applied either parallel to the c axis or in the ab plane.

III. RESULTS AND DISCUSSION

A. SQUID magnetometry

Figure 1 shows the isothermal magnetization curves measured at temperatures of 1.75 and 300 K in the field range of -10 kOe $< H < +10$ kOe for five samples of proton-bombarded graphite; premeasured data for the virgin samples were subtracted. It is the magnetic moment rather than the magnetization density that is shown in Fig. 1 for the latter can only be approximately estimated because of spatial inhomogeneities created by bombardment. The damaged volume of the graphite samples, i.e., the part of the sample subjected to the irradiation and where the magnetization presumably resided, was calculated by the SRIM simulation.[38] For the proton energy of 225 keV, the penetration depth in graphite is about 1.5 μm (0.85 μm for He^+); thus, the damaged volume is $\sim 3 \times 10^{-6}$ cm^3- the same for any fluence- and its weight is approximately 6 μg. A measured magnetic moment of 1×10^{-6} emu roughly corresponds to 0.15 emu/g (0.15 A m^2 kg^{-1}) of the average magnetization density in

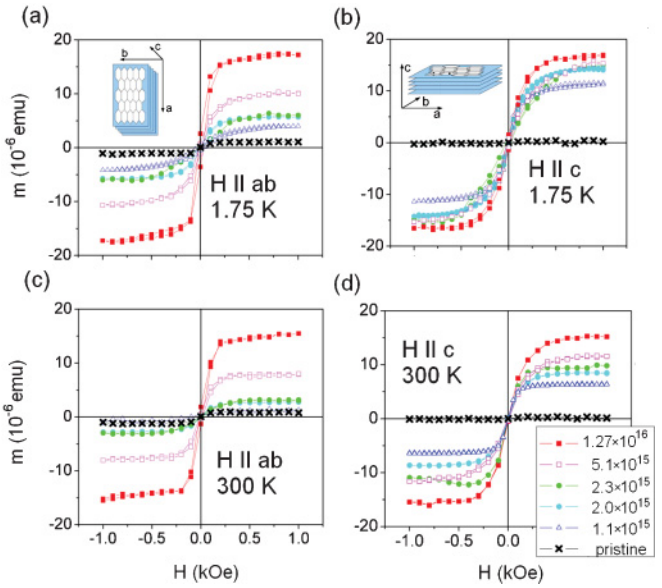

FIG. 1. (Color online) Hysteresis loops measured for the HOPG implanted with different doses of 225-keV energy protons at 1.75 K (a, b) and at 300 K (c, d). The magnetic field is applied parallel to the ab plane (a, c) or parallel to the c axis (b, d).

the damaged volume, and we use these approximate values in Fig. 2. The experimental data show that the magnetic moment at saturation is controlled by the total dose; however, the dose dependence of the saturation moment is different for the two orthogonal magnetic field directions as shown in Fig. 2(a). In Fig. 2(b), we plot the ratio of the saturation magnetization in orthogonal directions for 1.75 K and room temperature. Substantial at low irradiation doses, the anisotropy vanishes at a dose of about 1×10^{16} ion/cm^2. Further increase in irradiation dose destroys magnetic ordering. The sample irradiated with the dose 1×10^{17} ion/cm^2 (not shown in Fig. 1) did not display any nonlinear magnetization. Another remarkable feature of the magnetization loops is that their shape differs for the two field orientations. When the field is parallel to the graphene plane, the saturation is achieved at lower fields as could occur in the crystals with an easy direction of magnetization. The curves shown in Figs. 1(a) and 1(c) saturate at about 2–3 kOe, whereas the curves in Figs. 1(b)

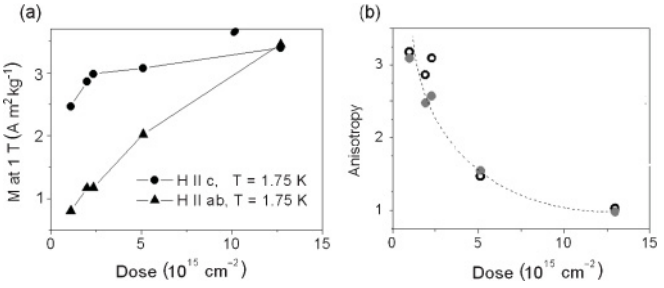

FIG. 2. Magnetic properties of proton-bombarded graphite versus irradiation dose (a) saturation magnetization for magnetic field applied parallel to the ab planes and parallel to the c axis, measurements at 1.75 K. (b) $M_{H||c}/M_{H||ab}$ ratio of saturation moments for magnetic field in orthogonal directions at 1.75 K (solid circles) and 300 K (open circles).

and 1(d) show saturation at higher fields, 3–5 kOe. The shape anisotropy is the same as that reported in Ref. 7, suggesting the presence of magnetic units which are oriented *perpendicular* to graphite planes. These observations question the role of hydrogen as a source of magnetism because the implanted hydrogen layer is situated *parallel* to the graphite surface.

Generally speaking, there are two scenarios to interpret the ferromagnetism induced by bombardment with hydrogen ions. The first one is that the irradiation implants hydrogen atoms, creating a hydrogen-rich layer, and the chemical activity of the implanted hydrogen leads to magnetism via this or that mechanism. The other possibility is that the implantation is of a secondary importance and the main effect is due to structural defects in the volume damaged by irradiation. To discriminate between the two scenarios, we have performed a comparative study of magnetism in HOPG samples of irradiated ions of hydrogen and chemically inert helium (He^+) with the same energy of the ions. The magnetization curves in Fig. 3 are qualitatively similar to those for the hydrogen bombardment. The saturation magnetization turns out to be even higher for helium ion irradiation, 6.5 A m^2 g^{-1} compared to 3.5 A m^2 g^{-1} in the case of protons, and this higher value was achieved at an order of magnitude lower dose than in the case of protons. These data are in line with another medium-energy-ion experiment,[29] where bombardment with carbon ions resulted in magnetization as high as 9 A m^2 kg^{-1}. Maximal values of magnetic moments for 225-keV He^+ irradiation correspond to the dose 2×10^{15} cm^{-1}, and increasing the He^+ dose leads to the vanishing of magnetism. The sample irradiated with He^+ at a dose of 1×10^{16} ion/cm^2 (not shown in Fig. 3) did not display nonlinear magnetization. The results in Figs. 1–3 suggest that chemistry of the projectiles is more than likely immaterial, and the irradiation-induced magnetic activity of graphite is due to structural damages. The absence of a dominant effect of hydrogen chemical activity on the damage structures in the irradiated graphite has previously been shown in the comparison of damage formation between deuterium and helium irradiation.[39]

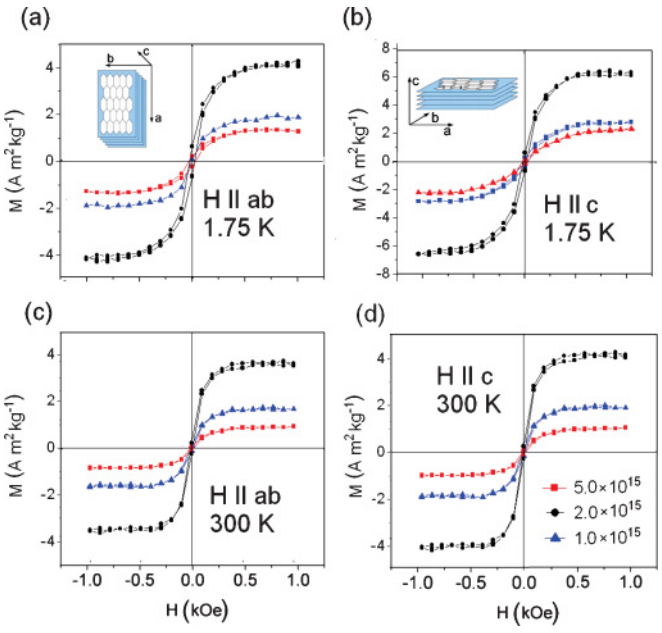

FIG. 3. (Color online) Hysteresis loops measured at 1.75 and 300 K for the HOPG implanted with different doses of 225-keV energy helium ions. Magnetic field is applied parallel (a) and perpendicular to the *ab* planes (b).

Another argument against the leading role of implanted hydrogen in magnetic properties of bombarded graphite is based on a simple fact that the number of implanted hydrogen atoms is much smaller than that of the displaced atoms in the damaged region. Assuming that every hydrogen atom introduced by irradiation saturates a carbon dangling bond resulting in a moment of 0.9–2.3 μ_B (Ref. 16) and provided that all moments interact ferromagnetically, the calculated magnetic signal will be an order of magnitude less than the measured magnetic signal. According to SRIM calculations,[38] the number of both vacancies and displaced carbon atoms is 8 times less for hydrogen than for helium ions with the same energy. Our experiments show that for the energy 235 keV the optimal dose for helium ions is about 2×10^{15} ion/cm^2 whereas for protons it lies between 1.27×10^{16} to 1×10^{17} ion/cm^2; thus the irradiation dose at which the magnetic signal reaches its maximum value is 10 times less for helium, in good accordance with the simulations. We thus conclude that the damaging process of ion-irradiated graphite causing the modification of its magnetic properties is dictated by the energy deposition rather than the nature of implanted ions. The role of molecular hydrogen present in the pristine sample and dissociating under the ion impact[35,40] is, however, not ruled out.

B. Atomic force microscopy

In order to understand the nature of structural modifications in bombarded graphite, we have performed atomic and magnetic force microscopy (AFM/MFM) studies of the sample surface. Measurements were performed in the atmosphere of dry nitrogen to avoid the effect of water absorption. Previous force microscopy studies of magnetic-irradiated graphite performed in Refs. 32 and 41 have shown that the MeV irradiation of HOPG leads to a swelling of the graphite surface with the apex in the beam center, height increasing with fluence. For the samples showing magnetism, the hill in the beam impact area was found to be from tens to hundreds of nanometers, whereas a magnetic signal was detected only in a narrow ring surrounding the irradiated spot.[12] In our medium-energy experiments the AFM measurements reveal quite different surface texture, and large statistics—hundreds of images taken across the bombarded spot on every sample—allow us to make definite conclusions. The whole irradiated area is covered with hillock-like protrusions (Fig. 4). The hillocks are not concentrated in the center of the beam, and the distribution of surface damages is even across the beam impact area, whereas the boundary between the irradiated and nonirradiated area is sharp and detectable [Fig. 5(a)].

The hillocks are occasionally randomly distributed but mainly concentrated along the straight lines protruding from the average surface level (Fig. 4), in accordance with the previous studies[42] which showed that the surface damage caused by medium energy ions is not uniform but appears in the form of groups. The tracks sometimes cross at the angles close to 60° or 90° indicating that the surface features reflect

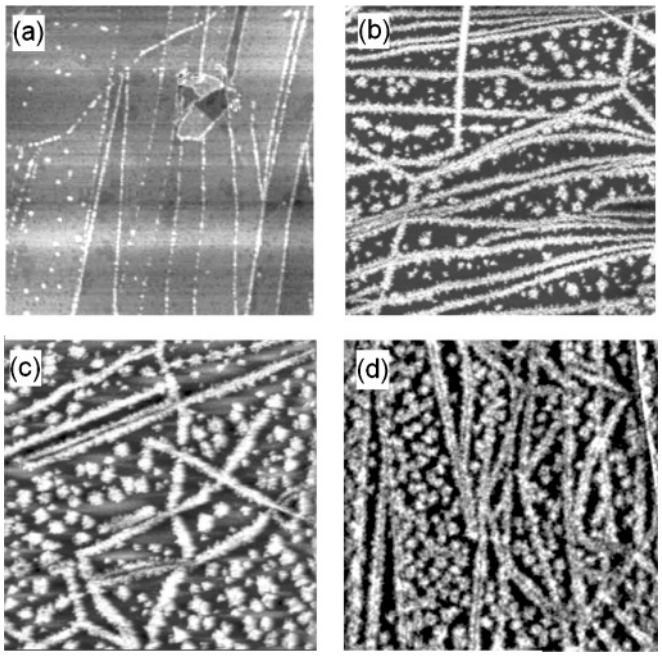

FIG. 4. Atomic force microscope images of proton-bombarded graphite with the scan size 10 × 10 μm. Dose: (a) 1 × 10^{15}; (b) 2 × 10^{15}; (c) 5 × 10^{15}; and (d) 1.27 × 10^{16} ion/cm^2, grayscale of 5 nm.

the intrinsic bulk mosaicity of graphite. The sources of damage in graphite are knock-on collisions followed by collision cascades initiated by the ejected atom creating interstitials, vacancies, and atom displacements.[43,44] The formation of regularly arranged surface patterns looks counterintuitive since the ion beam is homogeneous, but can be understood recalling that the simulations of damage production, e.g., SRIM code[38] do not take into account sample crystallinity and subsequent kinetics. In the crystalline regions the ions undergo low angle scattering events which results in generation of primary

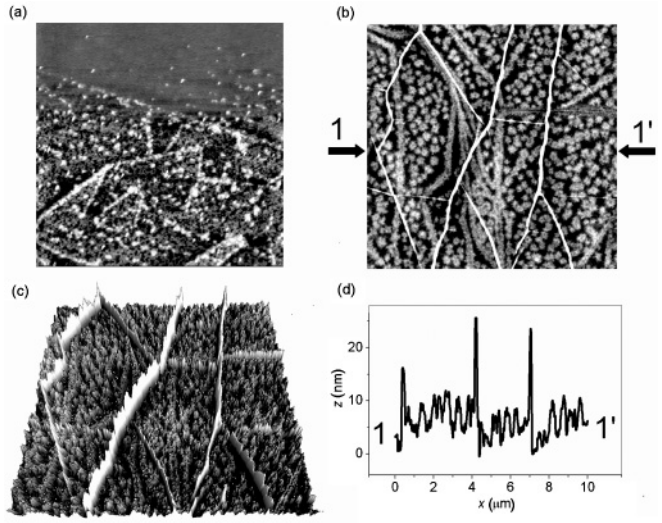

FIG. 5. Atomic force microscope images of proton-bombarded graphite. (a) Boundary of irradiated spot, dose 1× 10^{15}, scan size 2.5 × 2.5 μm. (b–d) Dose is 5 × 10^{15} ion/cm^2, scan size 10 × 10 μm. (b), 2D image; (c) 3D image; (d) line scan between the points 1 and 1′.

displacements whereas in the defective regions the ion-target interaction is dominated by large angle scattering events between the projectiles and the target atoms leading to the creation of damage cascades and the lateral broadening of the damage profile.[45] The damage is initially concentrated at the vertical grain boundaries of HOPG [Fig. 4(a)] and is followed by the damage accumulation, which is observed as progressive broadening of the lines in Figs. 4(a) to 4(d). Local raising of the surface does not result from sputtering but should be attributed to internal stresses which develop in the volume surrounding the ion track as damages and lattice defects are created by the collision processes.[46] Extended intergrain boundaries hinder the propagation of cascades and store radiation-induced defects.[47] Moreover, the defects can migrate away from their parent cascades to be absorbed at sinks such as grain boundaries.[48]

It should be stressed that the initial graphite surface is flat and most of the AFM 10 × 10 μm images taken before the ion irradiation do not reveal any steps. Occasionally, the steps on the initial surface were found, typically 1–3 nm in height.[50] A clear difference between the flat and featureless nonirradiated region and the textured irradiated spot shown in Fig. 5(a) confirms that the surface features develop at the places of *hidden* grain boundaries, buried underneath and propagating along the *c* axis of the graphite crystal. Figures 5(b)–5(d) demonstrate the scan obtained on the surface which apparently had step edges before the irradiation. The hillocks in the vicinity of the steps are higher than those appearing between the steps; they appear as distinct white lines in Fig. 5(b) and as sharp walls in Fig. 5(c) which is a three-dimensional version of Fig. 5(b). The line scan taken between the arrows 1 and 1′ [Fig. 5(d)] confirms that sharp spikes appear at the step edges whereas smaller linear features are created at the initially flat surface. Thus, the patterns on the irradiated HOPG surface reveal highly defective vertical planes created around the vertical grain boundaries of graphite. The two-dimensional AFM images obtained for protons and helium ions with the same energy and dose are very similar but they differ in the *z* direction: the height of the protrusions is 2 to 4 times higher for He^+ than for H^+ (Ref. 49).

C. Magnetic force microscopy

For the magnetic force measurements a two-pass technique was employed: the topography was imaged using the tapping mode, and magnetic force image of the same area was captured with the lift mode (lift height 50 nm) by mapping shifts in cantilever resonant frequency. Prior to acquiring an image, the scanning probe was magnetized with a permanent magnet. After obtaining the image, the tip was taken away, magnetized in the opposite direction, and returned to the same position. We minimized the contribution of electrostatic effects to the image by varying the voltage bias[50] and the contribution of capacitive and damping effects by tuning the speed and feedback gains.[7] To ensure that the produced images are of magnetic nature, the tip magnetization was reversed 5 times, and two of the measurements are shown in Fig. 6. The lift mode response of the samples is represented as a two-dimensional map with dark and bright areas. The repulsive interaction shifts the resonance frequency toward higher values which is encoded

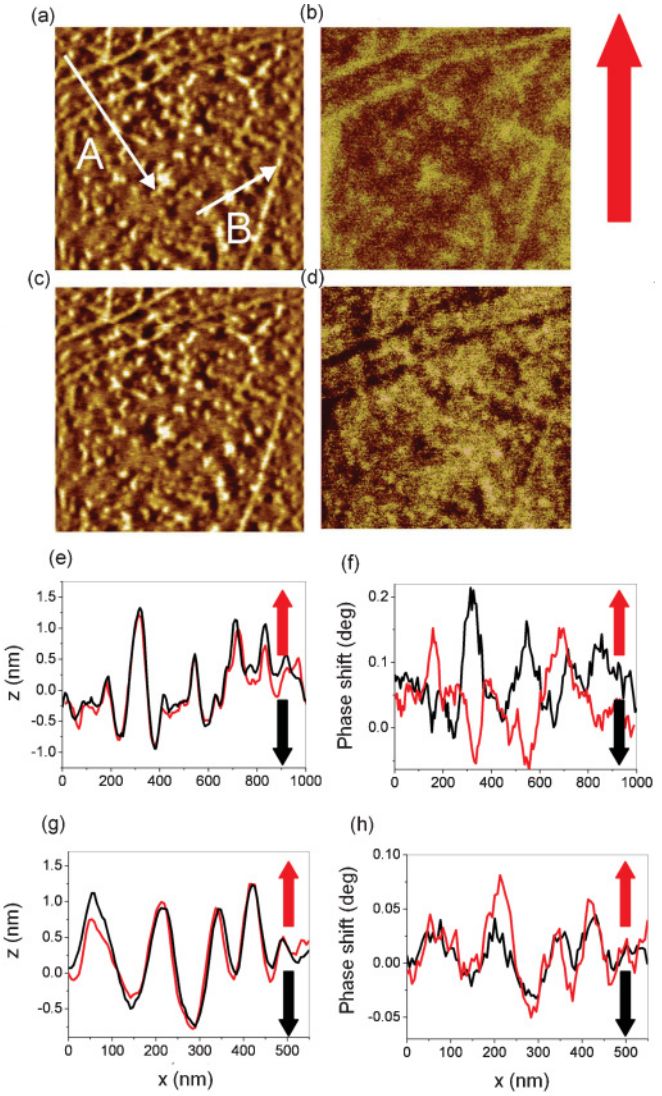

FIG. 6. (Color online) MFM measurements for two directions of tip magnetization. (a, c) Tapping mode topography; (b, d) frequency shift images (magnetic signal) obtained in the same area. Image parameters: scan area, 2×2 μm; lift height, 50 nm; AFM z range = 3 nm; MFM z range = 0.5°. (e, h) Topography profiles and frequency shift images as a function of the tip position along the white lines A and B in panel (a).

with a bright contrast in the phase detection. Similarly, a shift to lower frequencies reveals an attractive tip-sample interaction, and the regions with attractive interaction are represented by dark contrast. Figures 6(a)–6(d) show topography (left panels) and magnetic (right panels) images. The images (a) and (b) were taken with the plus tip magnetization (into the graphite surface), whereas the images (c) and (d) were taken with minus (out of the graphite surface) magnetization. As the tip magnetized into the graphite surface plane, nearly all topographic features show bright contrast, similar to the results on pristine HOPG (Ref. 7). After the magnetization direction was reversed to the out-of-plane one, some of the features produced a dark phase contrast on the line defects pointing out that the net magnetic moment stayed in the same direction.

Not all signals measured in the MFM were sensitive to the reversal of the tip magnetization. Whereas several linear structures are seen in the topographical image, only two line defects in the upper part of Figs. 6(a)–6(d) give well-defined magnetic responses changing the bright to dark appearance. On several other line defects the effect is present but less pronounced, whereas the lift mode signal did not change the sign and magnitude on the point defects. The above-mentioned phenomena are clearly seen on the lift mode signal profiles along the lines marked by A and B. Whereas the topography images [Figs. 6(e) and 6(g)] are nearly the same for two directions of tip magnetization (minor discrepancies are due to the difficulties with finding exactly the same place after the tip remagnetization), the phase shift images [Figs. 6(f) and 6(h)] are different. The A profile crosses the line defects, and the signal is strongly dependent on magnetization direction, whereas the B profile crosses only the point defects, and the phase signal is similar for both magnetizations.

Turning to the interpretation of the data obtained from bulk (SQUID) and local (MFM) magnetic measurements, we first note that the hillocks themselves are about 1 nm high and their magnetic contribution is unlikely significant. In our view, nonlinear in a magnetic field ferromagneticlike magnetization loops of the irradiated graphite samples are due to spin polarized structural defects, probably of the type analyzed in Refs. 13–27, the unpaired spins of which interact via the Heisenberg exchange establishing long-range magnetic order. The key observation in this paper is that the magnetic properties are anisotropic and that the degree of anisotropy varies with the irradiation dose. Since the exchange interaction does not select any preferable direction of the ordered spins, the anisotropy calls for more ingredients to interpret the data. We believe that the spin-orbital interaction, which naturally leads to a magnetic anisotropy of crystalline d ferromagnets like iron, cannot account for the data: Being of a relativistic origin, it is expected to be very weak in materials made of such a light element like carbon,[51] and even if operational, the randomness of the environment due to structural disorder is expected to average out the favorable directions locally selected by the spin-orbital interaction. Then, the only available anisotropic interaction is the magnetic dipole-dipole interaction or, in other words, the magnetostatic effects: the spins correlated via the Heisenberg exchange interaction select their common direction to minimize their magnetic energy eliminating stray magnetic fields as much as possible. The magnetostatics selects a spin axis adjusted to the spatial configuration of spins and leads to magnetic anisotropy (due to the geometric demagnetization factor).

D. Raman spectroscopy

Additional information about the nature of structural damages which give rise to induced magnetic activity of graphite comes from the fact that the dependence of induced magnetic moment versus irradiation dose shows a maximum after which magnetism quickly vanishes.[29,30] Although it is tempting to ascribe the vanishing of magnetism to complete destruction of the structure, our Raman spectroscopy studies show that this is not the case: Induced magnetism falls at a

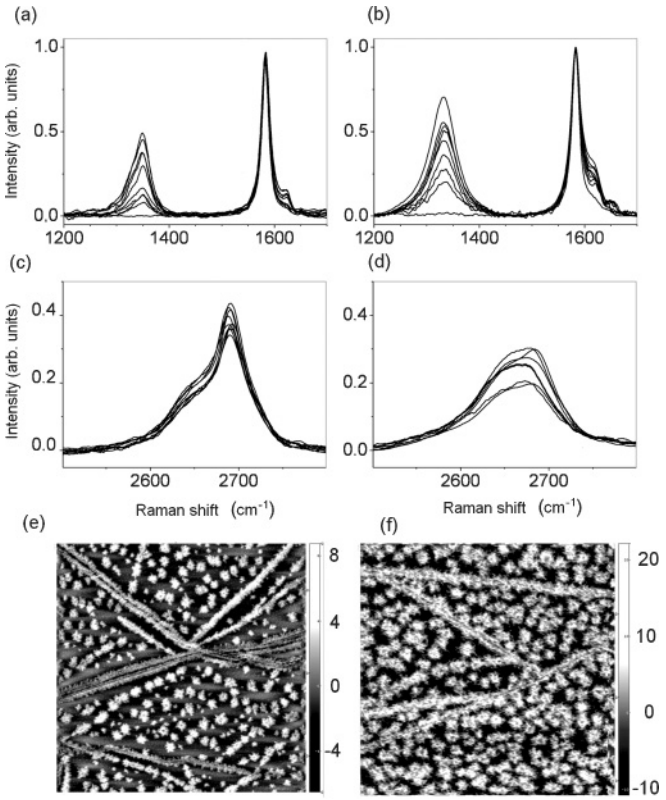

FIG. 7. Raman spectra of He^+-bombarded samples with the energy 225 keV and the dose of 1×10^{15} cm^{-2} (a, c) and 1×10^{16} cm^{-2} (b, d). AFM images of the samples (e, f). Window is 10×10 μm; grayscale values are in nm.

dose which is an order of magnitude smaller than the dose triggering the onset of amorphization.

Raman scattering spectra were collected with a micro-Raman Renishaw spectrometer equipped with a notch filter. The laser power was limited to 0.5 mW/cm^2 in order to avoid any amorphization and thermal relaxation. The beam was focused in the sample with a 50× objective which performed a 1-μm-diameter spot size. Figure 7 compares the Raman spectra of He^+-irradiated samples: "magnetic" ones irradiated with the dose 1×10^{15} ion/cm^2 and "nonmagnetic" ones irradiated with the dose 1×10^{16} ion/cm^2. We collected the spectra from different points of the samples and observed a spatial dependence of the peaks' intensity ratio [Figs. 6(a)–6(d)]: even on highly disordered samples some points corresponded to pristine graphite. This observation is in line with the AFM images [Figs. 7(e) and 7(f)], whereas multiple Raman curves confirm that the alternation of the damaged and undamaged regions is preserved deep in the bulk, within the laser beam penetration depth.

At low irradiation doses the first-order Raman spectrum exhibits the double-peaked spectrum, and the relative intensity of the D line (around 1350 cm^{-1}) with respect to the G mode (around 1580 cm^{-1}) varies as the inverse of the coherence length L_a of the cooperatively scattering graphitic domain and is used for the determination of this parameter.[52] At sufficiently high doses the disorder region around an ion trajectory undergoes crystalline-to-amorphous transformation[42] which is characterized by a bond angle disorder.[53] This process is detected by the onset of the rapid increase in both D and G linewidth and the appearance of a broad asymmetric line at around 1500 cm^{-1}. In Raman spectroscopy studies of ion-irradiated graphite it was shown that the transformation to an amorphous structure is abrupt and occurs at the critical fluence which varies with the mass of the implanted ion and its energy.[54] The critical fluence decreases with increase of projectile mass, in agreement with our experiments. As the critical fluence increases with energy, we can predict that the experiments with lower energy projectiles will require lower fluence for optimal magnetization. Comparing the spectra of "magnetic" and "nonmagnetic" samples, we notice that the D/G ratio for the "magnetic" samples reaches 0.5 ($L_a \sim$ 9 nm), whereas for the "nonmagnetic" one it reaches 0.7 ($L_a \sim 6.5$ nm). The absence of peak broadening shows that the amorphization threshold is not observed in the Raman spectra of both samples.

The second-order Raman spectra are even more sensitive than the first-order spectra for monitoring the threshold for the formation of the heavy lattice damage.[55] While the D/G ratio, i.e. the concentration of in-plane defects in both samples does not differ too much [Figs. 6(a) and 6(b)], we observe the qualitative difference between the out-of-plane defects through the changes in the second-order spectra [Figs. 6(c) and 6(d)]. The shape of the 2D band around 2700 cm^{-1} tells us that the "nonmagnetic" sample shows true, strong disorder, i.e., loss of turbostratic stacking: the 2700 cm^{-1} doublet starts to coalesce into a single broad peak. This is an indication of strongly perturbed Bernal stacking with a significant number of c-axis translation faults.[55] On the contrary, the spectrum of the "magnetic" He^+-bombarded sample has a two-peak shape which is typical for the 2D band in three-dimensional graphite samples. Our findings are in line with the high-resolution transmission electron microscope studies which have shown that during irradiation graphite easily loses its in-plane crystallographic order while hardly losing its layered structure.[56]

This observation confirms the expectations that stacking sequence plays a major role in graphite magnetism. Several theoretical groups,[13,16,25,57] following the work of Lieb on the Hubbard model,[58] came to the conclusion that the property that determines the magnetic behavior of the lattice is its bipartite nature. Searching for the origin of a sublattice unbalance, theory found out that hydrogen chemisorption or vacancy-interstitial recombination occurs more readily for the atoms in certain positions.[59] Thus, Bernal stacking provides the intrinsic discriminating mechanism[14] which creates the difference between the numbers of defects in two sublattices. Recent scanning tunneling microscopy experiments, complemented by tight-binding calculations,[15] revealed that the electronic resonance at the Fermi energy is different for the vacancies in different sublattices, suggesting that even randomly created vacancies could be the source of magnetic ordering provided that the Bernal stacking is preserved.

IV. SUMMARY

We have observed ferromagneticlike magnetization loops in highly oriented graphite samples irradiated by protons and helium at various irradiation doses. The impurity analyses as well as the dose dependence of the saturation magnetization

exclude any significant parasitic impurity contribution to the magnetic data. The magnetization curves are anisotropic, differing for an applied magnetic field in- and out-graphene planes. Anisotropy of magnetic properties for graphite is well known, both for the case of diamagnetism[60] and for intrinsic ferromagnetic signals.[7,10] However, for bombarded samples it has not been reported earlier; on the contrary, isotropy of the induced magnetic moment for high-energy bombardment was emphasized.[11] Similar anisotropy of the magnetization curve shapes were reported for nonirradiated graphite with high density of grain boundaries.[7] The latter observation was interpreted as due to the presence of the grain boundaries propagating along the *c* axis of the graphite crystal and creating vertical planes of defects, magnetostatic considerations choosing in-vertical-plane spin orientation. Our results, being qualitatively similar to those of Ref. 7, differ quantitatively: in our case magnetization values are several orders of magnitude higher. Nevertheless, we believe that the same physical picture is realized in our crystals at low irradiation doses where, as seen from the MFM-images, the defects are mainly concentrated on the vertically oriented grain boundaries. The enhanced magnetization in our irradiated samples can be attributed to a higher defect and, therefore, higher spin concentration on the grain boundary planes. This physical picture has been verified by the observation of a local stray field near linear defects by means of magnetic force microscopy.

Our data show that chemically inert helium is an efficient projectile for inducing magnetism in graphite. From this fact we conclude that the degree of a projectile chemical activity is not of primary importance and that the induced magnetism in bombarded graphite is primarily controlled by lattice defects generated by the irradiation. Medium-energy helium ions generate 8 times more isolated point defects (vacancies and interstitials), and the fluence for optimal magnetization is an order of magnitude less. The anisotropy of magnetic properties and the magnetism itself vanish at high irradiation doses. Our Raman studies reveal that the degradation of magnetic ordering at large irradiation doses occurs much earlier than graphite amorphization but coincides with the destruction of graphene sheet stacking. The evidence accumulated in our experiments supports the opinion that magnetism is linked to defects of graphite planes, i.e., vacancies, and the property that determines the magnetic behavior of graphite is the bipartite nature of its lattice.

ACKNOWLEDGMENTS

We thank P. Esquinazi for valuable advice during the experiments and T. Enoki for discussions. The authors acknowledge financial support from the EC FP6 “Ferrocarbon” project and from the Swedish Research Council.

*tatiana.makarova@physics.umu.se

[1] O. Volnianska and P. Boguslawski, J. Phys. Condens. Matter **22**, 073202 (2010).
[2] M. Stoneham, J. Phys. Condens. Matter **22**, 074211 (2010).
[3] A. Sundaresan and C. N. R. Rao, Nano Today **4**, 96 (2009).
[4] T. L. Makarova and F. Palacio, *Carbon Based Magnetism* (Elsevier, San Diego, 2006).
[5] Y.-W. Son, M. L. Cohen, and S. G. Louie, Nature (London) **444**, 347 (2006).
[6] O. V. Yazyev and M. I. Katsnelson, Phys. Rev. Lett. **100**, 047209 (2008).
[7] J. Cervenka, M. I. Katsnelson, and C. F. J. Flipse, Nat. Phys. **5**, 840 (2009).
[8] M. Sepioni, R. R. Nair, S. Rablen, J. Narayanan, F. Tuna, R. Winpenny, A. K. Geim, and I. V. Grigorieva, Phys. Rev. Lett. **105**, 207205 (2010).
[9] O. V. Yazyev, Rep. Prog. Phys. **73**, 056501 (2010).
[10] P. Esquinazi, A. Setzer, R. Hohne, C. Semmelhack, Y. Kopelevich, D. Spemann, T. Butz, B. Kohlstrunk, and M. Losche, Phys. Rev. B **66**, 024429 (2002).
[11] P. Esquinazi, D. Spemann, R. Hohne, A. Setzer, K.-H. Han, and T. Butz, Phys. Rev. Lett. **91**, 227201 (2003).
[12] H. Ohldag, T. Tyliszczak, R. Hohne, D. Spemann, P. Esquinazi, M. Ungureanu, and T. Butz, Phys. Rev. Lett. **98**, 187204 (2007).
[13] Y. Ma, P. O. Lehtinen, A. S. Foster, and R. M. Nieminen, New J. Phys. **6**, 68 (2004).
[14] O. V. Yazyev, Phys. Rev. Lett. **101**, 037203 (2008).
[15] M. M. Ugeda, I. Brihuega, F. Guinea, and J. M. Gomez-Rodriguez, Phys. Rev. Lett. **104**, 096804 (2010).
[16] P. O. Lehtinen, A. S. Foster, A. Ayuela, A. Krasheninnikov, K. Nordlund, and R. M. Nieminen, Phys. Rev. Lett. **91**, 017202 (2003).
[17] X. Yang, H. Xia, X. Qin, W. Li, Y. Dai, X. Liu, M. Zhao,Y. Xia, S. Yan, and B. Wang, Carbon **47**, 1399 (2009).
[18] H. Lee, Y. Miyamoto, and J. Yu, Phys. Rev. B **79**, 121404 (2009).
[19] K. Kusakabe and M. Maruyama, Phys. Rev. B **67**, 092406 (2003).
[20] O. V. Yazyev and M. I. Katsnelson, Phys. Rev. Lett. **100,** 047209 (2008).
[21] K. Sawada, F. Ishii, M. Saito, S. Okada, and T. Kawai, Nano Lett. **9**, 269 (2009).
[22] W. Li, M. Zhao, Y. Xia, R. Zhang, and Y. Mu, J. Mater. Chem. **19**, 9274 (2009).
[23] O. V. Yazyev and L. Helm, Phys. Rev. B **75**, 125408 (2007).
[24] R. Faccio, H. Pardo, P. A. Denis, R. Y. Oeiras, F. M. Araujo-Moreira, M. Verissimo-Alves, and A. W. Mombru, Phys. Rev. B **77**, 035416 (2008).
[25] L. Pisani, B. Montanari, and N. M. Harrison, New J. Phys. **10**, 033002 (2008).
[26] H. H. Lin, T. Hikihara, H.-T. Jeng, B.-L. Huang, C.-Y. Mou, and X. Hu, Phys. Rev. B **79**, 035405 (2009).
[27] E. Castro, M. Lopez-Sancho, and M. Vozmediano, New J. Phys. **11**, 095017 (2009)
[28] M. A. Ramos, J. Barzola-Quiquia, P. Esquinazi, A. Munoz-Martin, A. Climent-Font, and M. Garcia-Hernandez, Phys. Rev. B **81**, 214404 (2010).
[29] Y. Xia, C. Song, T. -W. Wang, D. Zhu, J. Gong, and Z. Zhu, Adv. Mater. **20**, 4679 (2008).

[30]J. Barzola-Quiquia, R. Hohne, M. Rothermel, A. Setzer, P. Esquinazi, and V. Heera, Eur. Phys. J. B **61**, 127 (2008).
[31]R. Hohne, P. Esquinazi, V. Heera, H. Weishart, A. Setzer, and D. Spemann, J. Magn. Magn. Mater. **320**, 966 (2008).
[32]K.-H. Han, D. Spemann, P. Esquinazi, R. Höhne, V. Riede, and T. Butz, Adv. Mater. **15**, 1719 (2003).
[33]D. Spemann, K.-H. Han, P. Esquinazi, R. Hohne, and T. Butz, Nucl. Instrum. Methods Phys. Res. Sec. B **219**, 886 (2004).
[34]J. Szczytko, P. Juszynski, L. Teliga, A. Stonert, R. Ratajczak, A. Korman, and A. Twardowski, Acta Phys. Pol. A **114**, 1387 (2008).
[35]J. Barzola-Quiquia, P. Esquinazi, M. Rothermel, D. Spemann, A. Setzer, and T. Butz, Nucl. Instrum. Methods Phys. Res. Sec. B **256**, 412 (2007).
[36]J. Barzola-Quiquia, P. Esquinazi, M. Rothermel, D. Spemann, T. Butz, and N. García, Phys. Rev. B **76**, 161403(R) (2007).
[37]K. W. Lee and C. E. Lee, Phys. Rev. Lett. **97**, 137206 (2006).
[38]J. F. Ziegler, J. P. Biersack, and U. Littmark, *The Stopping and Range of Ions in Matter* (Pergamon, New York, 1995).
[39]K. Niwase and T. Tanabe, J. Nucl. Mater. **203**, 56 (1993).
[40]M. Dubman, T. Shiroka, H. Luetkens, M. Rothermel, F. J. Litterst, E. Morenzoni, A. Suter, D. Spemann, P. Esquinazi, A. Setzer, and T. Butz, J. Magn. Magn. Mater. **322**, 1228 (2010).
[41]D. Spemann, K. Schindler, P. Esquinazi, M. Diaconu, H. Schmidt, R. Höhne, A. Setzer, and T. Butz, Nucl. Instrum. Methods Phys. Res. Sec. B **250**, 303 (2006).
[42]P. J. Zhai, Y. X. Xing, Y. Zhang, S. L. Feng, Y. X. Kang, X. W. Tang, Y. G. Wang, W. J. Zhao, and S. Yan, Radiation Measurements **28**, 97 (1997).
[43]M. S. Dresselhaus and R. Kallish, *Ion Implantation in Diamond, Graphite and Related Materials* (Springer, New York, 1992).
[44]F. Banhart, Rep. Prog. Phys. **62**, 1181 (1999).
[45]A. Kieslich, H. Doleschel, J. P. Reithmaie, A. Forche, and N. G. Stoffel, Nucl. Instrum. Methods Phys. Res., Sec. B **99**, 594 (1995).
[46]L. Porte, C. H. de Villeneuve, and M. Phaner, J. Vac. Sci. Technol. **9**, 1064 (1991).
[47]S. G. Psakhie, K. P. Zolnikov, D. S. Kryzhevich, A. V. Zheleznyakov, and V. M. Chernov, Cryst. Rep. **54**, 1002 (2009).
[48]D. Bacon, F. Gao, and Y. Osetsky, Nucl. Instrum. Methods Phys. Res. Sec. B **153**, 87 (1999).
[49]T. L. Makarova, A. L. Shelankov, I. T. Serenkov, and V. I. Sakharov, Phys. Status Solidi B **247**, 2988 (2010).
[50]T. L. Makarova and K. H. Han, Phys. Status Solidi B **244**, 4138 (2007).
[51]D. Huertas-Hernando, F. Guinea, and A. Brataas, Phys. Rev. B **74**, 155426 (2006).
[52]F. Tuinstra and J. L. Koening, J. Chem. Phys. **53**, 1126 (1970).
[53]K. Takahiro, A. Teraia, S. Oizumia, K. Kawatsura, S. Yamamoto, and H. Naramoto, Nucl. Instrum. Methods Phys. Res. Sec. B **242**, 445 (2006).
[54]B. S. Elman, M. Shayegan, M. S. Dresselhaus, H. Mazurek, and G. Dresselhaus, Phys. Rev. B **25**, 4142 (1982).
[55]H. Wilhelm, M. Lelaurain, E. McRae, and B. Humbert, J. Appl. Phys. **84**, 6552 (1998).
[56]T. Tanabe, S. Muto, and K. Niwase, Appl. Phys. Lett. **61**, 1638 (1992).
[57]M. P. López-Sancho, F. de Juan, and M. A. H. Vozmediano, Phys. Rev. B **79**, 075413 (2009).
[58]E. H. Lieb, Phys. Rev. Lett. **62**, 1201 (1989).
[59]O. V. Yazyev, I. Tavernelli, U. Rothlisberger, and L. Helm, Phys. Rev. B **75**, 115418 (2007).
[60]P. A. Thrower, D. C. Nagle, and W. S. Horton, J. Appl. Cryst. **6**, 347 (1973).